




Comparison of the charge-crystal and charge-glass state in geometrically frustrated organic conductors studied by fluctuation spectroscopy

Tatjana Thomas , Tim Thyzel, Hungwei Sun, and Jens Müller*
Institute of Physics, Goethe University Frankfurt, 60438 Frankfurt (M), Germany

Kenichiro Hashimoto 
*Department of Advanced Materials Science, University of Tokyo, 277-8561 Chiba, Japan
 and Institute for Materials Research, Tohoku University, 980-8577 Sendai, Japan*

Takahiko Sasaki 
Institute for Materials Research, Tohoku University, 980-8577 Sendai, Japan

Hiroshi M. Yamamoto
Institute for Molecular Science, Okazaki, 444-8585 Aichi, Japan



(Received 11 February 2022; accepted 2 May 2022; published 10 May 2022)

We present a systematic investigation of the low-frequency charge carrier dynamics in different charge states of the organic conductors θ -(BEDT-TTF) $_2$ $MZn(SCN)_4$ with $M = \text{Rb, Tl}$, which result from quenching or relaxing the charge degrees of freedom on a geometrically frustrated triangular lattice. Due to strong electronic correlations these materials exhibit a charge-ordering transition, which can be kinetically avoided by rapid cooling resulting in a so-called charge-glass state without long-range order. The combination of fluctuation spectroscopy and a heat pulse method allows us to study and compare the resistance fluctuations in the low-resistive quenched and the high-resistive charge-ordered state, revealing striking differences in the respective noise magnitudes. For both compounds, we find strongly enhanced resistance fluctuations right at the metal-insulator transition and a broad noise maximum in the slowly cooled charge-crystal state with partly dominating two-level processes revealing characteristic activation energies.

DOI: [10.1103/PhysRevB.105.205111](https://doi.org/10.1103/PhysRevB.105.205111)

I. INTRODUCTION

Recently, the formation of non-equilibrium metastable states when quenching charge degrees of freedom in condensed matter has attracted great interest [1]. Such a new state has been discussed in the organic conductors θ -(BEDT-TTF) $_2$ $MM'(SCN)_4$, where BEDT-TTF represents bis-ethylenedithio-tetrathiafulvalene (in short: ET) and $MM'(SCN)_4$ a monovalent anion with $M = (\text{Rb, Cs, Tl})$ and $M' = (\text{Co, Zn})$ [1–4]. These quasi-two-dimensional charge-transfer salts consist of an alternating structure of conducting layers with the $[(\text{ET})_2]^+$ molecules separated by insulating anion layers $[MM'(SCN)_4]^-$, where the charge transfer of two donor ET molecules to one acceptor molecule results in a quarter-filled (hole) conduction band. Due to strong electronic correlations the systems often exhibit a charge-ordered (CO) ground state, which can be described within the framework of the extended Hubbard model [5] under consideration of the nearest-neighbor lattice site interaction V in addition to the on-site Coulomb repulsion U [6]. However, it was found that the first-order CO transition can be kinetically avoided by rapid cooling leading to a so-called charge-glass state which lacks long-range order [2]. This state had been

interpreted in purely electronic terms by considering the frustration of charges due to the geometric arrangement of the ET molecules on an anisotropic triangular lattice within the conducting layer. Therefore, a suitable parameter to characterize the degree of frustration is the ratio of the inter-site Coulomb interactions V_2/V_1 along different crystallographic axes (see Appendix 1), which can be altered either by pressure or by chemical variations of the anion atoms M and M' [7]. This parameter has a severe influence on the critical cooling rate $|q_c|$ required to avoid charge ordering, where for the compounds with orthorhombic crystal structure a clear systematic is found, in which a stronger frustration leads to a higher charge-glass forming ability and therefore to lower critical cooling rates [1,3]. In the monoclinic compound θ -(ET) $_2$ TlZn(SCN) $_4$, in short θ_m -TlZn, the large anisotropy of the triangular lattice and thus low geometric frustration results in a high critical cooling rate $|q_c| > 50$ K/min [4], whereas in the orthorhombic system θ -(ET) $_2$ RbZn(SCN) $_4$, in short θ_o -RbZn, with medium frustration a charge-glass state is reported for cooling rates $|q_c| \gtrsim 5$ K/min [2]. The two compounds exhibit different CO patterns, i.e., a diagonal pattern for θ_m -TlZn and a horizontal one for θ_o -RbZn, where the monoclinic θ_m -TlZn approximates a system where the effects are purely electronic in nature [4]. This is in agreement with the development of varying CO patterns by considering different electron-phonon interactions [8,9].

*j.mueller@physik.uni-frankfurt.de

Fluctuation (noise) spectroscopy has proven to be a powerful tool to study the low-frequency dynamics of the charge carriers in molecular metals providing information on inhomogeneous current distributions, slow dynamics due to a glassy freezing of structural or electronic degrees of freedom, or the slowing down of the charge carrier kinetics in the vicinity of a critical endpoint, see, e.g., Refs. [10,11] and references therein. Indeed, for the title compounds θ -(ET)₂MM'(SCN)₄, measurements of the resistance noise above the metal-insulator transition in θ_o -RbZn, θ_o -CsZn, and θ_m -TlZn revealed slow and heterogeneous dynamics [2,4,12,13], which are ascribed to vitrification or glassy freezing of the dynamics of charge clusters upon approaching the glass-transition temperature from above. Most remarkably, the process of charge crystallization in the supercooled state was found to be very similar to that of conventional glass-forming liquids. Studying charges on a geometrically frustrated lattice in molecular metals can therefore help to better understand the physics of glasses in general [4,14]. Contrary to the interpretation of the charge-glass formation in purely electronic terms, recent thermal expansion combined with resistance fluctuation spectroscopy measurements on the highly frustrated θ_o -CsZn and θ_o -CsCo have provided evidence for a *structural* glassy transition at $T_g \approx 90$ –100 K [15]. This and strong structural changes at the metal-insulator transition in θ_o -RbZn [7,16,17] raise the question, to what extent structural degrees of freedom are involved in the development of different charge states in the less geometrically frustrated compounds and highlights the need for further investigations of the novel charge-glass state.

In this work, we extend the previous studies of the charge carrier dynamics, which were restricted to temperatures above the metal-to-insulator transition, to a systematic investigation of all three different charge states, namely the charge-liquid (CL) state at high temperatures $T > T_{CO}$, where the charge is homogeneously distributed in space, the ordered charge-crystal (CC) state for $T < T_{CO}$ for slow cooling and the metastable charge-glass (CG) state, when CO is kinetically avoided by fast cooling. The different states are investigated in orthorhombic θ_o -RbZn as well as in the monoclinic variant of θ_m -TlZn, which exhibit a different strength of charge frustration and electron-phonon coupling. For both compounds, we find strongly enhanced and slow resistance fluctuations right at the transition into the charge-ordered phase as well as a broad noise maximum below T_{CO} . In θ_o -RbZn, the fluctuations in the charge-crystal state are dominated by two-level processes characterized by slow and heterogeneous dynamics. In addition, deviations from a quadratic current dependence of the power spectral density of current fluctuations are observed, which coincide with the onset of nonlinear IV curves in the charge-ordered state, whereas for θ_m -TlZn a quadratic scaling of the noise was observed. In both systems, the comparison of the charge carrier dynamics in the quenched CG state reveals a much lower noise magnitude than that of the CC state.

II. EXPERIMENT

Single crystals of θ -(ET)₂MM'(SCN)₄ were grown by electrochemical crystallization [7]. θ -RbZn crystals were

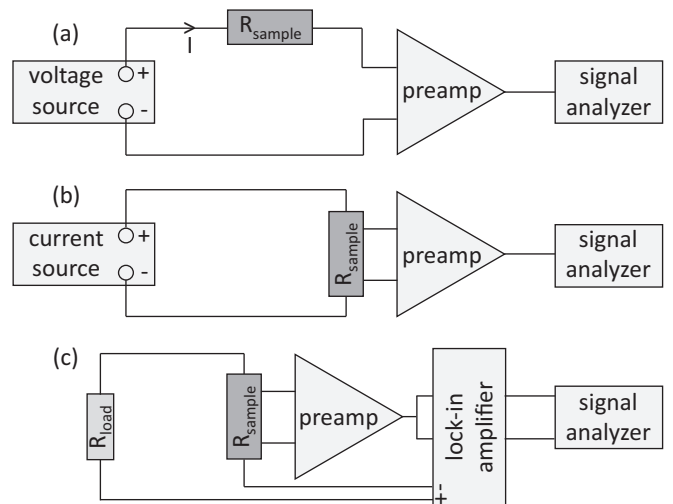


FIG. 1. Different setups for fluctuation spectroscopy: (a) Two-point DC setup (\circ) for measurements of current (conductance) fluctuations in high-impedance samples, (b) four-point DC setup (\square), and (c) four-point AC setup (\triangle) for measurements of voltage (resistance) fluctuations in more conductive samples. The fluctuating signal in each case is fed into a signal analyzer (SR785) to obtain the noise power spectral density (PSD). The data symbols shown in the figures below indicate which setup has been used.

grown with an improved method that does not use 18-crown-6 ether. Rb(SCN) and Zn(SCN)₂ were solubilized by using MeOH/1,1,2-Trichloroethane (1:9 v/v) as a solvent in the electrochemical process. Resistance measurements have been performed parallel to the conducting layers in a DC configuration, for which 10- or 25- μ m-thick gold wires were attached to the crystal using carbon paste. Due to the large variation of the samples' impedances, sometimes of several orders of magnitude, upon cooling down from room temperature, the measurement setup for fluctuation spectroscopy, schematically shown in Fig. 1, was varied such that four-terminal AC and DC techniques were used to measure voltage fluctuations and a two-terminal DC conductance method for measuring current fluctuations, see Refs. [10,11] for more detailed information.

A constant DC voltage or current was supplied by Keithley sourcemeters (K2400 or K2612), whereas a lock-in amplifier (Stanford Research Systems SR830) combined with a load resistor was used for the AC technique. For the two-point conductance method the sample is connected in series with a current amplifier (NF CA5350 or Keithley K428), where the internal resistance determines the gain and transforms the current to a voltage signal. For the four-terminal setups a preamplifier (SR560) was used. The main advantage of the AC technique is the minimization of the preamplifier's own, extrinsic $1/f$ noise contribution by choosing a suitable excitation frequency to operate in the "eye" of the preamplifier's noise figure [18]. The fluctuating signal is further processed by a signal analyzer (Stanford Research Systems SR785), which calculates the fast Fourier transform and provides the power spectral density (PSD) $S_{V,I}(f)$ of the voltage or current fluctuations. Usually this quantity exhibits a quadratic dependence on the applied voltage or current in

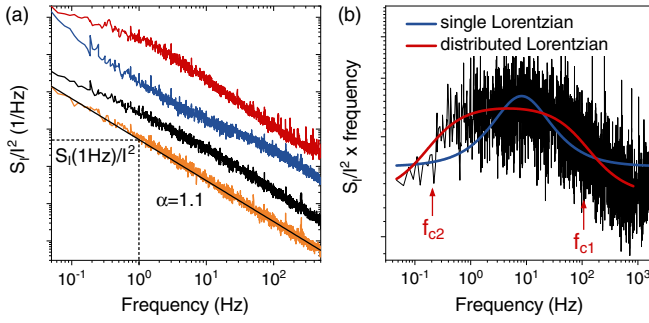


FIG. 2. (a) Typical noise spectra either of $1/f$ -type or superimposed with a Lorentzian contribution for selected temperatures in θ_o -RbZn (sample #1). (b) Comparison of the single and distributed Lorentzian model, where the latter can better reproduce the line width of the measured spectrum.

the ohmic regime [19,20] so that the normalized PSD S_V/V^2 or S_I/I^2 , conveniently taken at 1 Hz, is used for analyzing the temperature-dependent noise magnitude on different samples. It was always ensured that the measured noise originates from the sample and not from the preamplifier or other external sources and that the normalized spectra of different techniques yield the same results, i.e., $S_V/V^2 = S_I/I^2 = S_R/R^2 = S_G/G^2$, where the indices denote voltage, current, resistance, and conductance, respectively. The observed noise spectra were either of pure $1/f$ -type or composed of underlying $1/f$ noise superimposed with a single or distributed Lorentzian contribution, exemplarily shown in Fig. 2(a) for a θ_o -RbZn sample at various different temperatures.

The noise PSD of a superposition of $1/f$ noise and a single Lorentzian contribution can be written as

$$\frac{S_R(f)}{R^2} f = \frac{A}{f^{(\alpha-1)}} + \frac{B}{4\pi^3} \frac{f}{f^2 + f_c^2}, \quad (1)$$

where A is the magnitude of the $1/f$ -noise contribution and α the frequency exponent, which corresponds to the slope in a double-logarithmic plot, i.e., $\alpha = -\partial \ln S_V(f)/\partial \ln f$. The amplitude of the Lorentzian contribution is determined by $B = (\Delta R/R)^2/(\tau_1 + \tau_2)$. The corner frequency f_c , where $f \times S_R(f)/R^2$ vs. f exhibits a maximum, is defined by $f_c = 1/(2\pi\tau_c) = 1/(2\pi)(1/\tau_1 + 1/\tau_2)$ with τ_1 and τ_2 describing the characteristic lifetimes of the states in a double-well potential with an energy barrier E_a that must be overcome. For a thermally activated process it is $f_c = f'_0 \exp[-E_a/(k_B T)]$ with an attempt frequency f'_0 . In some cases, we found that the line width of the superimposed two-level fluctuations was broader than that of a single Lorentzian, see example shown in Fig. 2(b). In this case, we employ the distributed Lorentzian model suggested in [2] for analyzing the spectra.

In order to realize the charge-glass state even for θ_m -TlZn with a large critical cooling rate, a heat pulse technique [21] was employed. Thereby the sample's resistance acts as a Joule heater ($P = RI^2$) and the sample is thermally coupled to the low-temperature heat bath, see Appendix 2. Starting at low temperatures, by applying a stepwise increasing heating current, the sample can be warmed up above T_{CO} in a controlled way by monitoring the two-point sample resistance. In order to prevent amplifying effects of the heating power when the

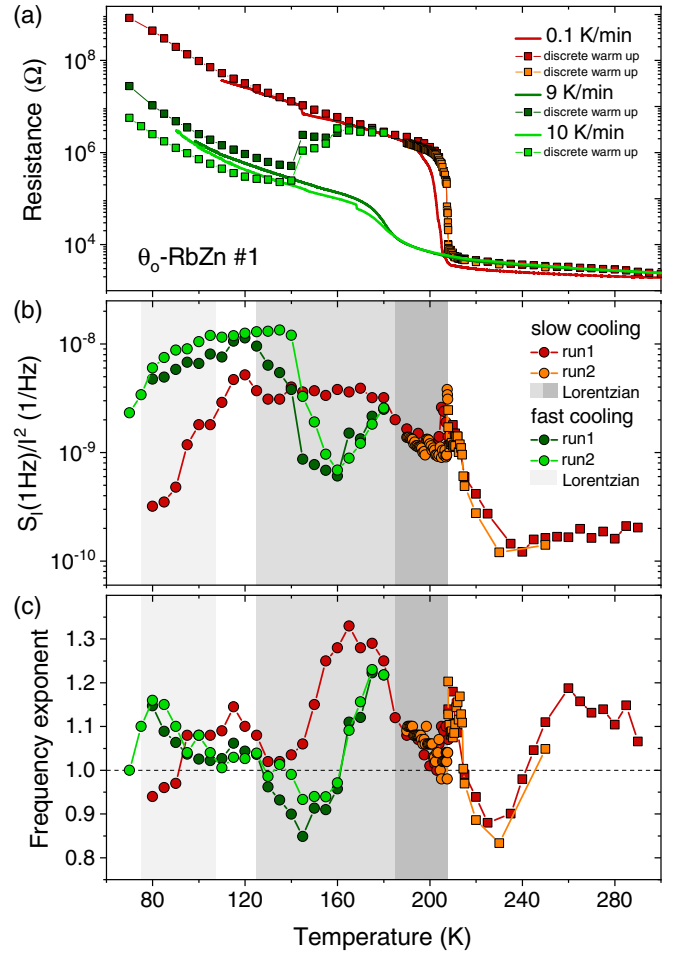


FIG. 3. (a) Resistance, (b) normalized current or voltage noise PSD, and (c) frequency exponent α of the $1/f^\alpha$ -noise contribution vs temperature of θ_o -RbZn (sample #1) for the slow- and fast-cooled state. Only the first term of Eq. (1) is evaluated here. The shaded areas mark the regions where additional, superimposed Lorentzian spectra emerge, see also Fig. 6 below. Different symbols mark different measurement techniques (see Experiment).

sample resistance decreases abruptly at the charge-ordering transition, a constant current rather than a voltage is applied. When switching off the heating current, the sample cools down very fast with an estimated lower limit of the cooling rate of $|q| \approx 700$ K/s near T_{CO} , resulting in a quenched charge state.

III. RESULTS AND DISCUSSION

A. θ -(ET)₂RbZn(SCN)₄

1. Cooling-rate-dependent resistance

The θ_o -RbZn compound with medium frustration shows a strong cooling-rate dependence of the resistance, as depicted in Fig. 3(a). For slow cooling with $|q| = 0.1$ K/min (solid red line), a CO transition from the CL into the CC phase occurs at $T_{CO} \approx 200$ K, which is accompanied by a sudden increase of the resistance by three orders of magnitude and a clear hysteresis upon warming up, typical for a first-order phase transition. For fast cooling with $|q| \approx 10$ K/min (solid

green lines) we observe a smooth continuation of the CL curve at T_{CO} which means that the sharp first-order transition is suppressed and a CG state is realized. However, although the absolute resistance value is at least two orders of magnitude smaller than in the ordered phase below T_{CO} , we still observe a broadened, step-like increase of the resistance below the transition region at $T \approx 180$ K, indicating that the critical cooling rate of 5 K/min reported in the literature [2] is too slow in our case. Analyses of the temperature-dependent resistance curves for slow and fast cooling by assuming an Arrhenius behavior at low temperatures (see Appendix 3) and comparing the ratio of respective activation energies with the literature [22,23] also support the hypothesis that the CO transition is not fully suppressed for the applied cooling rate. This may be due to the higher quality of the present samples, grown with an improved method, a notion that is corroborated by the observation that disorder introduced by x-ray irradiation has a strong impact on the CG forming ability [24]. Another possible explanation are size effects, as in Ref. [25] it was reported that a smaller sample size of the systems IrTe_2 and $\theta_o\text{-RbZn}$ causes a higher degree of supercooling, which also affects the critical cooling rate for quenching the system.

For the present compound, we were able to extend previous noise measurements, which were limited to the CL state [2,4], to both the ordered CC phase below T_{CO} and the metastable CG state and compare the low-frequency charge carrier dynamics in these states. The resistance and noise measurements shown in Figs. 3(a)–3(c), respectively, were performed during warming up the sample in discrete temperature steps. Due to the peculiar electron (cluster) dynamics and crystallization for the fast-cooled state, at 145 K the resistance starts to relax back to the ordered CC phase upon warming and approaches the slowly cooled curve at 180 K. The crystallization dynamics of electrons in this temperature regime has been studied in detail [4,14], surprisingly revealing—despite the quantum nature of electrons—the same nucleation and growth processes that characterize conventional glass formers.

An important issue in the CO phase are nonlinear IV curves with power-law exponents $b \equiv d \ln(I)/d \ln(V)$ up to 1.6 [red squares in Fig. 4(a)], which were suggested to originate in electric field-induced unbinding of thermally activated electron-hole pairs [22,23]. These intrinsic nonlinear effects also have been discussed in Refs. [17,26,27] and assigned to the current-induced melting of CO, which can develop from the avalanche-like creation of many electron-hole pairs. X-ray diffuse scattering experiments [26] have shown that the $q_2^2 = (0, k, 1/2)$ modulation, whose three-dimensional (3D) order is associated with the metal-insulator transition, is unstable against strong electric current, resulting in a decrease of the number of domains which exhibit the local q_2^2 order. In contrast to the CC state, the CG state [green squares in Fig. 4(a)] shows almost linear IV characteristics above about 100 K before it starts to deviate from ohmic behavior upon further cooling, in accordance with [23], where the nonlinearity for fast cooling sets in at lower temperatures than for slow cooling, which was attributed to the larger activation energy in the CC state. Since the IV curves were taken upon warming up the sample in discrete steps, the degree of nonlinearity approaches that of the slow-cooled CO state during relaxation of the quenched state at $T \approx 180$ K. If the nonlinear IV

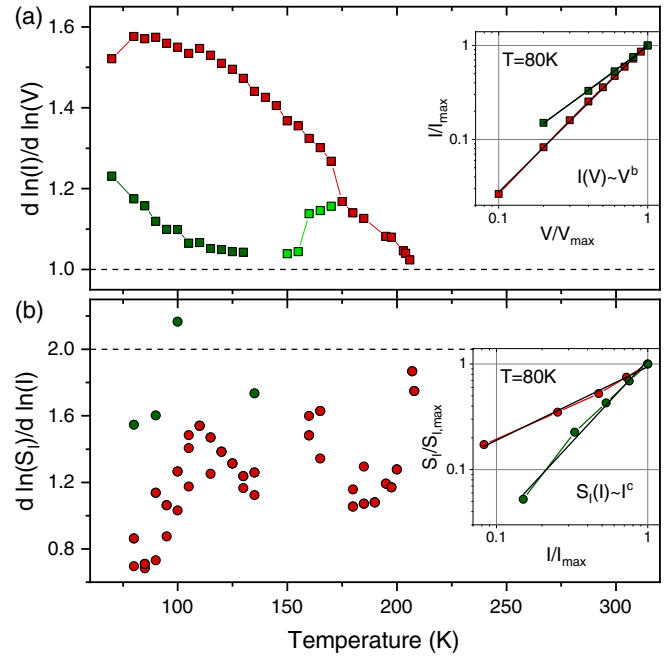


FIG. 4. Power-law exponents of the (a) nonlinear IV curves and of the (b) noise PSD in dependence of the current, $d \ln(S_f)/d \ln(I)$, of $\theta_o\text{-RbZn}$ (sample #1). The dashed lines indicate ohmic behavior and quadratic current dependence of the noise, which is valid above the charge-ordering transition. Insets show the IV curves (upper inset) and the current-dependent PSDs (lower inset) in a double-logarithmic plot at $T = 80$ K for the slow- (red) and fast-cooled state (green).

curves were caused by Joule heating, by keeping the power roughly constant the nonlinearity would be larger for higher temperatures compared to lower T , since less power is needed to heat parts of the sample above the transition temperature to the metallic state when the system is closer to T_{MI} [28]. The implications of these nonlinearities for the noise measurements are discussed below.

2. Resistance noise in the slow-cooled state

The noise measurements which were performed in a two-terminal (circular symbols) and four-terminal (squares) DC configuration agree well as demonstrated by their overlap for the temperatures where both setups have been used. A comparison of the noise results for the CC and CG states reveals important differences in the respective charge carrier dynamics [see Figs. 3(b) and 3(c) for magnitude and frequency exponent, respectively]. Another striking observation is a sharp and pronounced peak in both the noise magnitude and the frequency exponent at the temperature of the transition from the CO to the CL phase upon warming at T_{CO} , see Figs. 3(b) and 3(c). Such an enhancement of the noise magnitude and strong shift of spectral weight to low frequencies ($\alpha > 1$) have been observed for another $\theta_o\text{-RbZn}$ sample (not shown) and may be related to fluctuations of microscopic entities which play a key role in phase transitions, also of first-order, in two dimensions [29].

Remarkably, the normalized noise PSD of the slowly cooled state (red and orange color) becomes strongly en-

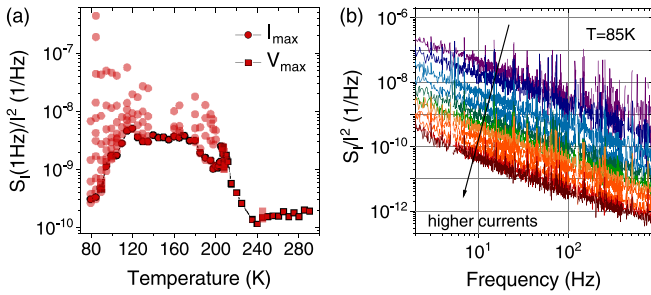


FIG. 5. (a) Normalized PSD taken at 1 Hz vs temperature for different currents of θ_o -RbZn (sample #1). Dark symbols indicate the values for the maximum current or voltage, transparent symbols represent the values for smaller currents and voltages. (b) Spectra for different currents are exemplarily shown for $T = 85$ K.

hanced already at temperatures $T \lesssim 230$ K, i.e., about 25–30 K above the transition [cf. the resistance $R(T)$], as compared to the rather flat behavior in the CL phase at higher temperatures. The rise of the noise magnitude upon approaching the transition from above is a clear signature of slowly fluctuating charge clusters as charge disproportionation has been observed already in the metallic phase above T_M [30,31]. This behavior continues upon cooling through T_{CO} down to $T \approx 160$ K, where a plateau develops. Along with this increase of the magnitude of the fluctuations we observe a concurrent change of the frequency exponent from $\alpha = 0.8$ at $T = 230$ K to $\alpha = 1.3$ at 160 K. This substantial shift of spectral weight to lower frequencies is in accordance with the freezing of the charge clusters' dynamics [2,4,14]. As pointed out above, note that superimposed on this broad evolution of the charge fluctuation dynamics to slower timescales are the sharp peaks in magnitude and frequency exponent at the phase transition T_{CO} . For lower temperatures $T \lesssim 120$ K the PSD apparently decreases again, accompanied by a frequency exponent α around 1, which implies a more homogeneous distribution of the relevant dynamic time scales.

At this point it is necessary to discuss the nonlinearities, described above for the resistance or conductivity, also for the PSD of the voltage or current fluctuations, which usually scale with the voltage or current squared [19,20], i.e., $S_I \propto I^2$. Interestingly, this scaling relation is not observed in the CC state, where the data can be described by $S_I \propto I^c$ with $c \approx 0.7$ –1.6. The power-law exponent $c \equiv d \ln(S_I)/d \ln(I)$ of the current-dependent PSD for the slow- (red) and fast-cooled (green) state is illustrated in Fig. 4(b). Since the nonquadratic noise is most pronounced in the charge-ordered phase, where also nonlinear IV curves in the time-averaged transport occur, the transport mechanism responsible for this nonlinearity may also influence the strength of fluctuations. The current-dependent normalized noise PSD S_I/I^2 makes it now difficult to compare its magnitudes at different temperatures, since the maximum applied current varied in the experiment (in order to keep the Joule power roughly constant and thereby avoid sample heating) as well as the strength of nonquadraticity of the noise varies as a function of temperature.

The PSD normalized to I^2 at 1 Hz evaluated for different currents is shown in Fig. 5(a). The value for the maximum applied current or voltage is indicated by the dark red cir-

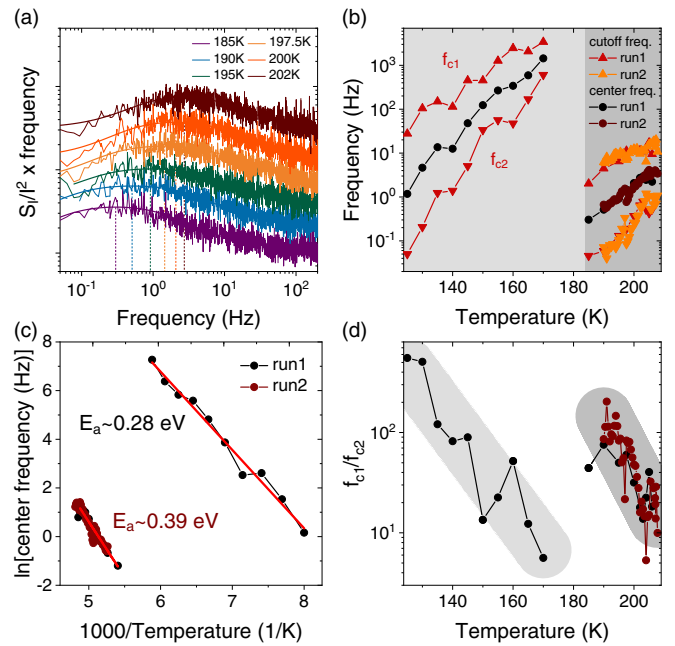


FIG. 6. (a) Examples of Lorentzian contribution superimposed on the $1/f$ spectra in the temperature region 125–205 K measured in the CC state of θ_o -RbZn. (b) f_{c1} and f_{c2} stands for the high- and low-frequency cutoffs, $f_0 = \sqrt{f_{c1}f_{c2}}$ for the center frequency. (c) Extracted energies from the center frequency and (d) line width of the distributed Lorentzian contribution.

cles and squares [cf. Fig. 3(b)], whereas the values for lower currents or voltages are represented by transparent symbols. By comparing $S_I/I^2(1\text{Hz})$ for different currents and temperatures, it can be seen that the strongest variation is below 120 K, also indicated by the small value of the power-law exponent c [Fig. 4(b)]. This is visualized in Fig. 5(b), where the normalized spectra measured at $T = 85$ K vary by almost three orders of magnitude. Therefore, we assign the strong decrease of the noise level with the maximum applied current at low temperatures ($T < 120$ K) to the nonquadraticity of the noise. The strong reduction of the noise PSD for higher currents might be caused by electric-field-induced free charge carriers, also responsible for the nonlinear IV characteristics [23], resulting in an enhanced number of fluctuators and therefore a lower overall noise level due to cancellation effects. Likewise, the current-induced melting of CO domains [17,26,27] may increase the number of conduction paths or the noisy volume. We note that nonquadratic noise has also been observed in other systems [32–34], see also Ref. [20]. A mathematical treatment of this phenomenon is given in Appendix 4.

3. Dominating two-level processes

In addition to the $1/f^\alpha$ fluctuations, we find superimposed Lorentzian contributions for temperatures $125 \text{ K} < T < T_{CO}$ for slow cooling, which implies one or a few dominant fluctuating processes. Hence, it should be noted that the values for $S_I(1 \text{ Hz})/I^2$ shown in Fig. 3(b) represent the underlying $1/f$ noise. The analysis of the non- $1/f$ contribution, fitted by a distributed Lorentzian model [2] [solid lines in Fig. 6(a)], reveals two different processes dominating the noise in the

temperature regions $125 \text{ K} \lesssim T \lesssim 185 \text{ K}$ and $185 \text{ K} \lesssim T \lesssim T_{\text{CO}}$ (gray shaded regions in Fig. 3).

From the high- and low-frequency cutoffs f_{c1} and f_{c2} we extract a center frequency $f_0 = \sqrt{f_{c1}f_{c2}}$ [black and brown symbols in Fig. 6(b)], which follows an Arrhenius law $f_0 \propto \exp[-E_a/(k_B T)]$, i.e., the frequency shifts to higher values for increasing temperatures as shown in Fig. 6(a). The corresponding activation energies E_a , which dominate the charge fluctuations in the CC phase, are 0.28 and 0.39 eV, cf. Fig. 6(c). One can speculate that these energies correspond to the energy barrier of the switching between metallic and insulating phases or between charge clusters with different local orders. From the ratio of the cutoff frequencies, shown in Fig. 6(d), we can see, that for both processes the line width f_{c1}/f_{c2} becomes broader for decreasing temperatures implying that the dynamics becomes more heterogeneous. Similar features of slow and heterogeneous dynamics were found in the CL state for different θ - MM' compounds [2,4,12,13] and were ascribed to the freezing of charges on the triangular lattice.

The observed two-level processes in the slow-cooled CC state with pronounced Lorentzian contributions may be attributed to electronic phase separation or phase coexistence near the first-order charge-ordering transition [35,36]. However, such processes are also observed in the CC phase even well below the metal-insulator transition. Possibly the switching of metallic and insulating clusters or of domains with different competing local orders persists even deeper in the insulating phase. An incomplete formation of charge order would explain the existence of slow and heterogeneous dynamics of charge clusters freezing in a glassy manner even below T_{CO} , originating from a small liquid (metallic) phase. Another possible origin of coexisting phases is a (current-induced) destabilization of the CO state, which alters the energies of the switching two-level processes, since in the slow-cooled state also nonlinear IV curves were observed.

4. Resistance noise in the partly quenched state

The noise level of the partly quenched state [green symbols in Fig. 3(b)] is about one order of magnitude higher at low temperatures but undershoots the slow-cooled curve at the temperature where relaxation begins. For further warming, the PSD monotonically increases and reaches the slow-cooled curve after completed charge crystallization. Notably, in the relaxation region, repeated noise measurements at a fixed temperature fall on one curve when normalizing the PSD to the actual resistance at that time. This means that, within the measuring time, the fluctuating processes do not change, although the resistance value changes. In contrast, the temperature has a strong influence on the noise, which monotonically increases with increasing T until the curve of the slowly cooled state is reached. A possible explanation are different nucleation mechanisms for the temperature regimes, as discussed in Ref. [14], where below the nose temperature of the time-temperature-transformation (TTT) diagram the fraction of CO domains remain undeveloped, whereas the resistance already increases with time. The coexistence of two competing local orders have been observed for intermediate cooling speed by x-ray diffuse scattering [26,37], where

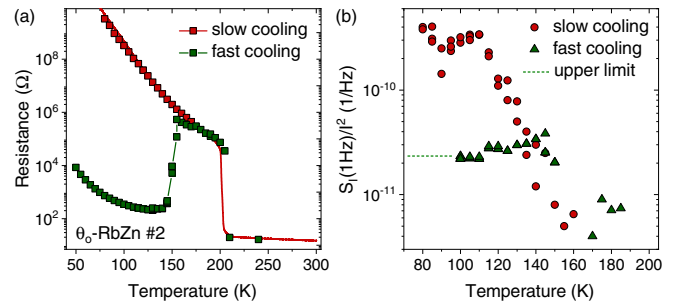


FIG. 7. (a) Resistance and (b) normalized PSD taken at 1 Hz of θ_o -RbZn (sample #2) for the slow- and fast-cooled state, which was generated by using a heat pulse.

heating leads to the growth of the thermodynamically stable $q_2' = (0, k, 1/2)$ modulation. We therefore assign the increase of the low-frequency fluctuations in the relaxation region to the crystallization process, where charge clusters start to grow and rearrange.

In the temperature region $75 \text{ K} \lesssim T \lesssim 105 \text{ K}$ we observe (single) Lorentzian spectra superimposed on the $1/f$ spectra. From the corner frequency, which follows an Arrhenius law, an energy of $E_a \approx 180 \text{ meV}$ is deduced, which is significantly lower than the energies observed for the CC state. Since the fast-cooled state at low temperatures is most likely a mixture of CC and CG phases, the higher noise magnitude might be due to an inhomogeneous current flow, which results in a small noisy volume and therefore leads to a large noise magnitude. Since the sample was cooled down with a continuous helium-flow cryostat with variable temperature insert (VTI), the maximum cooling rate in the relevant temperature range was limited to $\approx 10 \text{ K/min}$. In order to compare the slow-cooled state with the fully quenched charge-glass state, a second sample of θ_o -RbZn was examined with the aid of a heat pulse method.

5. Resistance noise in the fully quenched state

Figure 7(a) shows the resistance of θ_o -RbZn, sample #2, for slow ($|q| = 0.1 \text{ K/min}$) (red) and fast cooling (green). The resistance values (square symbols) were measured when warming up the sample in discrete temperature steps after slow and fast cooling (employing the heat pulse technique). In comparison with the first sample, here the charge-ordering transition is sharper and the total increase of the resistivity amounts to ≈ 9 orders of magnitude from room temperature to 75 K, implying a better sample quality or the appearance of size effects [25] (see above), as sample #2 has a larger volume ($V_2 \approx 3 \times 10^7 \mu\text{m}^3$) than sample #1 ($V_1 \approx 3 \times 10^6 \mu\text{m}^3$). The application of the heat pulse technique with $|q| \gtrsim 700 \text{ K/s}$ leads to a full suppression of the transition and to huge differences in the resistance by many orders of magnitude. This is corroborated by the ratio of activation energies of the slow- and fast-cooled states assuming an Arrhenius law (see Appendix 3), in agreement with Ref. [23].

For this sample, measurements of the resistance fluctuations were only possible below the transition, probably due to the small absolute resistance at high temperatures resulting in a low overall noise magnitude. The comparison of the PSD

of the slow- and fast-cooled state for $T < T_{CO}$ is shown in Fig. 7(b). Below $T \approx 130$ K the charge-glass state shows a significantly smaller noise magnitude as compared to the CC state. At the temperature, where the resistance relaxes back to the CC phase, the noise measurements yield similar results. Below 100 K the resistance fluctuations of the quenched state were too small compared with the noise floor of our experimental setup at these temperatures indicated by the dashed green line giving an upper limit of the PSD. Therefore, no crossing of the curves is to be expected and the enhanced noise level in the fast-cooled state for the first sample is probably caused by a mixture of different phases because of not fast enough cooling rates. These findings are in agreement with the results on θ_m -TiZn, which are discussed in the next section.

B. θ -(ET)₂TiZn(SCN)₄

1. Cooling-rate-dependent resistance

θ_m -TiZn shows a low degree of frustration and therefore a large critical cooling rate is required to quench the charge-ordered state. The system variant with monoclinic crystal structure studied here [4] exhibits a charge-ordering transition at $T_{CO} \approx 175$ K with clear hysteresis, see Fig. 8(a) (red line). In the temperature region around 130 K the slope of the resistance curve increases for decreasing temperatures, possibly due to a change of the transport mechanism, e.g., a stronger localization of the charge carriers, and another resistance anomaly is seen at around 115 K in the CC state.

Due to the large anisotropy of the triangular lattice in θ_m -TiZn and thus a strong tendency for charge crystallization, we again used a modified heat pulse technique as described in Ref. [21] to achieve cooling rates larger than $|q_c| \approx 50$ K/min required to realize the CG state. The comparison of the resistance curves for slow cooling (red curve) and for the resistance after applying a heat pulse and warming up again (green curve) is shown in Fig. 8(a). Although the quenched state has been reached resulting in two distinct resistance curves of the CG and CC states, the difference only amounts to about one order of magnitude in the region $T = 80$ –120 K which is much smaller than for the θ_o -RbZn compound, which may be ascribed to the different position in the phase diagram [4]. (The steeper slope dR/dT just above the transition indicates a more insulating behavior.) For the quenched state, at $T \gtrsim 110$ K, the resistance starts to relax back to the CC state and relaxation is completed at about 160 K.

2. Resistance noise in the slow-cooled state

Noise measurements were performed during warming up the sample in discrete temperature steps for both charge states, which revealed spectra of $1/f$ -type for the whole temperature range. For temperatures $T < T_{CO}$, a two-terminal DC current noise (circular symbols) as well as a four-terminal DC voltage noise technique (square symbols) was used, whereas in the charge-liquid state a four-terminal AC voltage noise method (triangular symbols) was more suitable. The normalized noise magnitude at 1 Hz for the slowly cooled state [red and orange symbols in Fig. 8(b)] is almost constant at high temperatures and reveals a pronounced increase starting just around 175 K, which coincides with the charge-ordering temperature. One

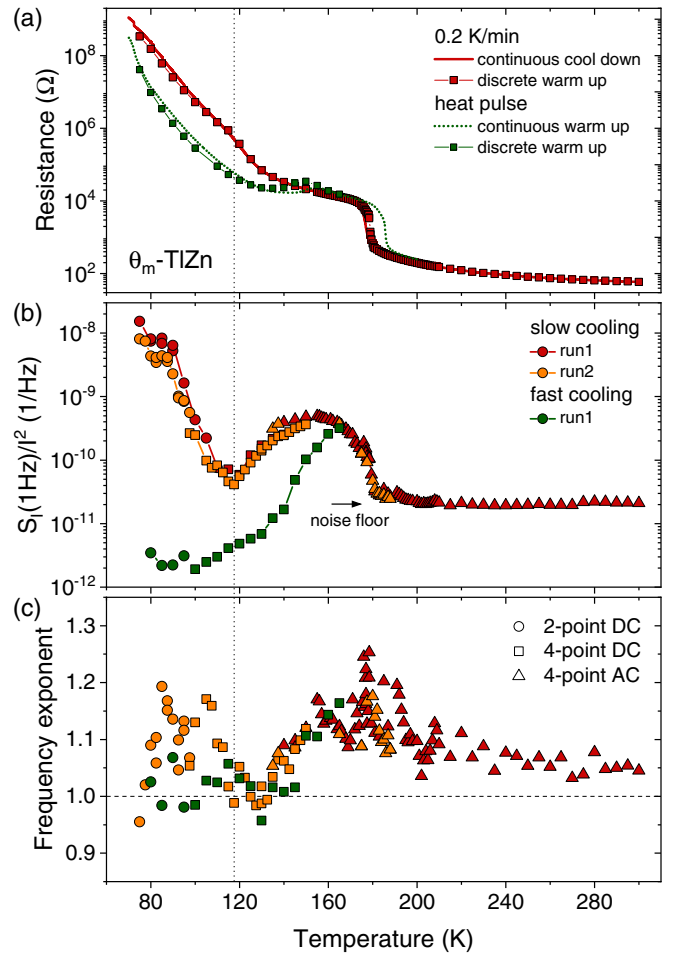


FIG. 8. (a) Resistance, (b) normalized PSD, and (c) frequency exponent of the $1/f$ spectra measured on θ_m -TiZn for the slow- (red) and fast-cooled state (green). The symbols mark different measurement techniques for fluctuation spectroscopy.

should note that the noise level above the transition is mainly limited by the noise floor of the experimental setup in this temperature region (marked by an arrow). Right at the first-order transition, again the frequency exponent is enhanced showing a peak structure similar to the behavior of θ_o -RbZn (Fig. 3). Below T_{CO} , in the CC phase the noise magnitude shows a broad maximum around $T \approx 150$ K, which concurs with the flat (plateau-like) resistance curve. This may indicate that a not yet fully completed charge order causes the strong resistance fluctuations. Below $T \approx 120$ K, coinciding with the resistance anomaly (marked by the dotted line), the noise PSD shows a sharp increase by almost three orders of magnitude upon further lowering the temperature. (The latter can be described equally well with an exponential function and a power-law behavior which implies a scaling $S_1/I^2 \sim R^\nu$ expected for a percolative system [38]; here, we find $\nu = 0.94$.) The frequency exponent of the $1/f$ spectra [Fig. 8(c)] shows enhanced values up to $\alpha \approx 1.3$ in the CO transition region and decreases as the noise magnitude approaches its minimum at $T \approx 120$ K. The strong increase of the noise level at low temperatures then is accompanied by larger values for α , although the curve progression varies between 1.0 and 1.2.

3. Resistance noise in the quenched state

The normalized PSD at 1 Hz for the quenched state [green symbols in Fig. 8(b)] is four orders of magnitude lower at the lowest measured temperature ($T = 75$ K) and increases gradually upon warming up the sample until it matches the noise level of the CC state after completed relaxation. Remarkably, in contrast to the resistance, which shows only small changes when comparing the relaxed and the quenched state, the resistance noise differs drastically, such that the less ordered, glassy electronic state is much more “quiet” regarding its low-frequency fluctuations. The frequency exponent is almost constant with $\alpha \approx 1$ for temperatures $T < 120$ K and increases up to 1.2 in the region of charge relaxation, where it coincides with the slowly cooled state. The resistance as well as the noise results have been reproduced for repeated measurements, which confirms that the sample was not modified by the large heating current and that switching between different charge states is reversible (also regarding the fluctuation dynamics), as demonstrated in Ref. [39] by exploiting this effect as phase-change memory function.

IV. CONCLUSION

We have investigated the low-frequency charge dynamics of different charge states in the organic conductors θ -(ET)₂MZn(SCN)₄ with $M = \text{Rb, Tl}$, which exhibit a varying strength of geometric frustration and electron-phonon coupling. We were able to compare the resistance and conductance noise PSDs in the CL state at high temperatures with those in both the CC and CG states at low temperatures. The compounds θ_o -RbZn and θ_m -TlZn, which exhibit a first-order transition at $T_{\text{CO}} \approx 200$ K and ≈ 175 K, respectively, show a strong increase of the resistance fluctuations when approaching the charge-ordering temperature from above for slow cooling. Right at the transition the noise magnitude as well as the frequency exponent show pronounced peaks indicating slow dynamics due to fluctuating microscopic entities being a signature of the first-order phase transition. In the CC state of θ_o -RbZn Lorentzian spectra superimposed on the $1/f$ background reveal slow and heterogeneous dynamics with characteristic energies of 0.28 and 0.39 eV. Accompanying nonlinear IV curves we observe nonquadratic noise, i.e., deviations from the usual quadratic current or voltage scaling of the PSD. A possible scenario is that higher electric fields induce additional free charge carriers or decrease the number of CO domains, which leads to a lower noise magnitude due to an increasing number of fluctuators or noisy volume. An open question is, if the current-dependent noise is partly caused by electronic ferroelectricity, which is reported to be induced by CO in combination with a small dimerization of the ET molecules [40,41]. A strong dependence of the PSD on the electric field was also observed in Ref. [42] and assigned to fluctuating polar clusters. The higher noise level of the fast-cooled state in θ_o -RbZn is probably caused by a mixture of CC and CG phases, since measurements on a second sample, where a heat pulse technique was used to fully suppress the CO transition, reveal a lower noise magnitude for the whole temperature range. This is in agreement with results on θ_m -TlZn where the CG state shows values of the PSD, which

are several orders of magnitude smaller compared to those of the CC state. Possible explanations for this are strongly inhomogeneous current paths in the insulating CC state, which reduces the noisy volume and therefore leads to an increase in the noise magnitude, whereas a smaller domain size in the CG state [2] leads to more homogeneous current flow through the sample. This could lead to much smaller energy scales of the dominating fluctuators in the CG state compared to the CC state meaning that the low-frequency fluctuations are dominant at lower temperatures. It is worth noting that a model of nonexponential kinetics by Dutta, Dimon, and Horn (DDH model) [43], based on independent thermally activated fluctuators distributed in energy, describes the temperature- and frequency-dependent $1/f^\alpha$ noise very well in highly frustrated θ_o -CsCo [15] and θ_o -CsZn [13]. However, it is not applicable for the samples discussed here exhibiting a charge-ordering transition. This may be interpreted in a sense that the charge dynamics in the CC state is rather governed by interacting clusters. Since the CG state for the less frustrated compounds show a different noise behavior than the one observed in θ_o -CsZn and θ_o -CsCo, which exhibits a structural glass transition [15], thermal expansion measurements are highly desirable to study the influence of structural degrees of freedom on the novel charge-glass state.

ACKNOWLEDGMENTS

We acknowledge support by the Deutsche Forschungsgemeinschaft (DFG, German Research Foundation) through TRR 288 - 422213477 (Project No. B02). This work was also supported by Grants-in-Aid for Scientific Research (KAKENHI) from MEXT, Japan (No. JP21H01793, No. JP20H05144, No. JP19H01833, and No. JP18KK0375), and Grant-in-Aid for Scientific Research for Transformative Research Areas (A) Condensed Conjugation (No. JP20H05869 and No. JP21H05471) from Japan Society for the Promotion of Science (JSPS).

We would like to acknowledge R. Murata for synthesizing single crystals of θ -RbZn.

APPENDIX

1. Crystal structure

The molecular arrangement of the donor molecules in θ -(ET)₂MM'(SCN)₄ with orthorhombic and monoclinic symmetries are shown in Fig. 9. The conducting layer within the a - c (left) and b - c plane (right) containing the BEDT-TTF molecules can be mapped on a triangular lattice with relevant inter-site Coulomb repulsions V_1 and V_2 . The degree of frustration determined by the anisotropy of the triangular lattice, V_2/V_1 , is higher for θ_o -RbZn ($V_2/V_1 = 0.87$) [3] compared with θ_m -TlZn ($V_2/V_1 = 0.8$) [4].

2. Heat pulse technique

To achieve large cooling rates in order to avoid the charge-ordering transition, a modified version of the heat pulse technique as described in Ref. [21] is used. In this method, the sample with resistance R acts as the heater itself, whereas the temperature of the bath (i.e., the massive copper block of

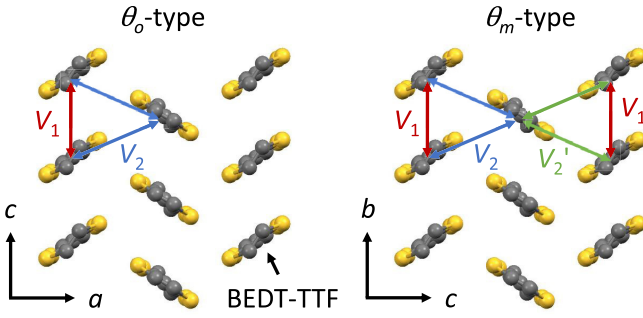


FIG. 9. Molecular arrangement of the orthorhombic (left) and monoclinic (right) θ -(ET)₂MM'(SCN)₄ within the conducting layers viewed along different crystallographic axes.

the sample holder in the cryostat) stays constant. By applying a stepwise increasing current, here supplied by a sourcemeter K2400, the Joule heat $P = RI^2$ is deposited in the sample, which heats up until it reaches the equilibrium temperature T_∞ determined by the coupling to the low-temperature heat bath. The reason for applying a constant current instead of a voltage lies in the negative resistance coefficient $dR/dT < 0$ at the transition, so that amplifying effects of the heating power can be avoided when the resistance always decreases during warming. By gradually increasing the current, the sample can be warmed up above the CO transition. It was always ensured that the equilibrium temperature is reached by waiting a few seconds before setting the higher current and monitoring the sample resistance by a voltmeter. When switching off the sourcemeter, the sample temperature relaxes back to the bath temperature with very high cooling rates under sufficient thermal coupling. The system can be described by a simple model [21], which is sketched in Fig. 10.

The sample with temperature T_s and specific heat C is thermally coupled to the heat bath with temperature T_{bath} through the thermal conductivity λ . The corresponding equation for the power balance is given by

$$P = C\dot{T}_s + \lambda(T_s - T_{\text{bath}}).$$

The solution of this differential equation is

$$T_s(t) = [T_s(t=0) - T_\infty] \exp\left(-\frac{\lambda}{C}t\right) + T_\infty,$$

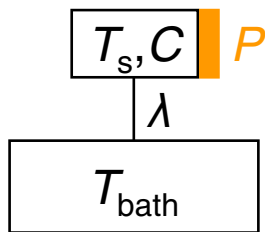


FIG. 10. Simple model for the thermal conductance in the heat pulse technique after Ref. [21]. The cold heat bath with constant temperature T_{bath} is indicated by the lower rectangle, whereas the sample with temperature T_s and specific heat C corresponds to the smaller rectangle. The Joule heat P (orange) is deposited by a large current flowing through the sample with resistance R .

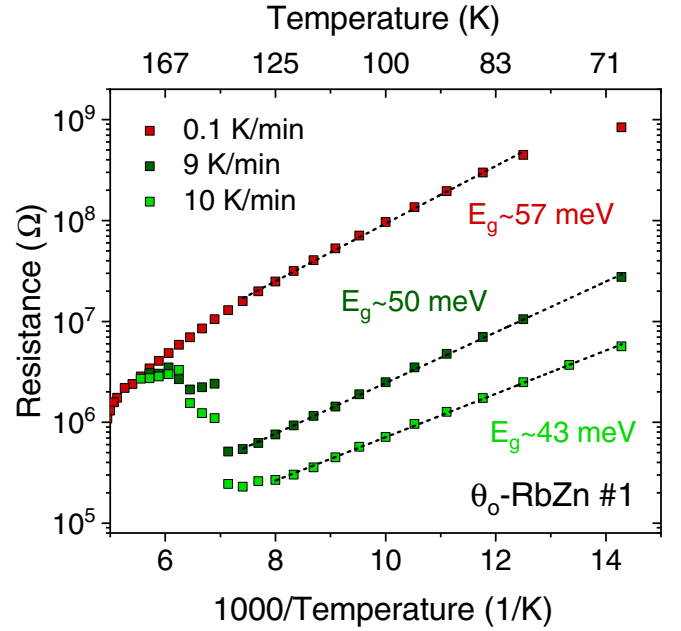


FIG. 11. Logarithmic resistance of θ_o -RbZn (sample #1) against the inverse temperature of the slow- (red) and fast-cooled (green) state.

with the equilibrium temperature $T_\infty = \lim_{t \rightarrow \infty} T_s(t) = \frac{P}{\lambda} + T_{\text{bath}}$. In order to obtain the temperature decay of the sample during fast cooling, we used a second sourcemeter K2400 to superimpose a small measuring current which does not lead to further warming of the sample. The fast resistance change after switching off the heating current can be determined by measuring the voltage drop with time using the buffer mode of the device. From the temperature-dependent resistance after warming up the quenched state, one in principle can extract $T(t)$ during fast cooling by matching $R(t)$ and $R(T)$. However, due to relaxation effects when warming up, this reference curve is missing in the transition region. From an underestimation of the temperature change ΔT and an overestimation of the time difference Δt , we find a cooling rate of $|q| = |\frac{\Delta T}{\Delta t}| \approx 700$ K/s as a lower limit.

3. Temperature dependence of the resistance

The temperature-dependent resistance of the θ_o -RbZn compound shows thermally activated behavior at low temperatures, i.e., $R = R_0 \exp[E_g/(k_B T)]$ with an energy gap E_g , as reported previously in the literature [22,23] (please note the factor of two in their definition, i.e., $E_g = \Delta_0/2$). The resistance was measured with a relatively low current or voltage to ensure almost linear (Ohmic) behavior. The logarithmic resistance of θ_o -RbZn against the inverse temperature is shown in Fig. 11 (sample #1) and Fig. 12 (sample #2) for the slow- (red) and fast-cooled (green) state.

The extracted energy gap at low temperatures of sample #1 yields $E_g = 57$ meV for the CO state. The energy gap for fast cooling should be much smaller according to Refs. [22,23], where $E_{g,\text{slow}}/E_{g,\text{fast}} \approx 2.46$. Here, however, we find a only slightly smaller value of 43–50 meV, which indicates that the CO transition is not fully suppressed. The application of

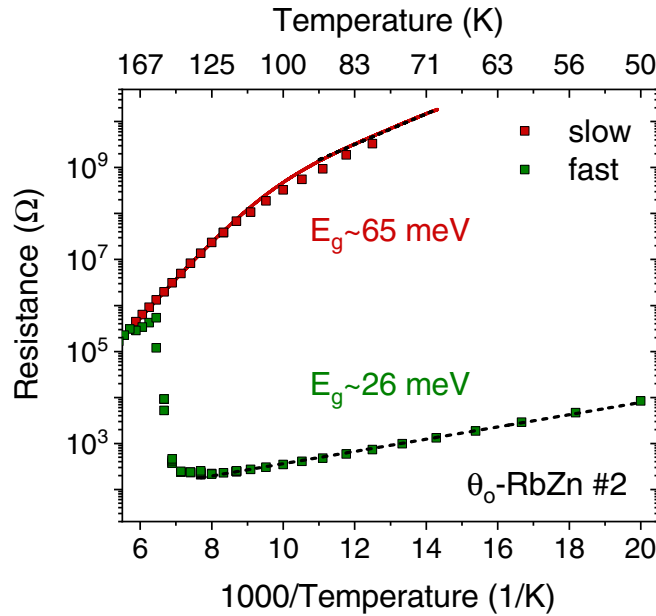


FIG. 12. Logarithmic resistance of θ_o -RbZn (sample #2) against the inverse temperature of the slow- (red) and fast-cooled (green) state after the application of a heat pulse.

the heat pulse technique on sample #2 leads to an activation energy of $E_g = 26$ meV, matching the value found in Ref. [44]. Thus the ratio of activation energies of the slow- and fast-cooled state is $E_{g,\text{slow}}/E_{g,\text{fast}} \approx 2.47$ (see Fig. 12) in agreement with Ref. [23], indicating the complete formation of the CG state.

4. Nonquadratic noise

To study the effects of nonlinear IV curves on the scaling relation of the noise, we consider the Hooge law [19], which is given by

$$S_I = \frac{\gamma_H I^c}{n\Omega f^\alpha}, \quad \text{with } c = 2,$$

where $\gamma_H \equiv \gamma$ is an empirical parameter (dimensionless for $\alpha = 1$). The current noise PSD under consideration of nonlinear IV curves with $I(V) \propto V^b$ is

$$S_I = \frac{\gamma I^2}{n\Omega f^\alpha} \propto \frac{\gamma (V^b)^2}{n\Omega f^\alpha}.$$

By inserting the value of the power-law exponent $b = 1.6$ for the slow-cooled state in θ_o -RbZn (sample #1) at 80 K [cf. Fig. 4(a)], one gets 3.2 for the voltage exponent, which does not match with the experimental findings of $c < 2$, cf.

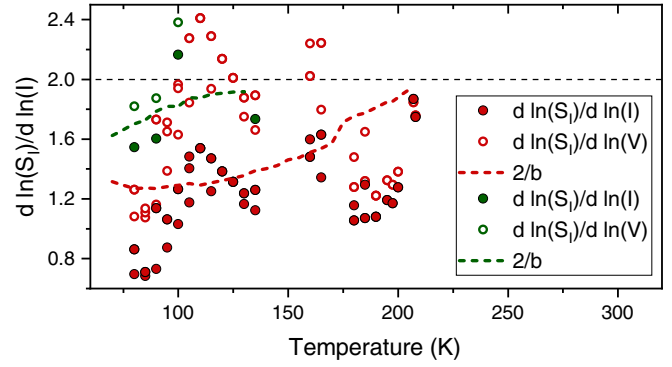


FIG. 13. Power-law exponents of the PSD in dependence of the current, $d \ln(S_I)/d \ln(I)$, (filled circles) as well as in dependence of the voltage, $d \ln(S_I)/d \ln(V)$ (empty circles), for the slow- (red) and fast-cooled state (green). The red and green dashed lines are the calculated values according to $c = 2/b$ assuming the Hooge law under consideration of nonlinear IV curves.

Fig. 4(b). Under the assumption that the Hooge law is valid for a constant applied voltage and that $V(I) \propto I^{1/b}$, one gets

$$S_I = \frac{\gamma V^2}{n\Omega f^\alpha} \propto \frac{\gamma I^{2/b}}{n\Omega f^\alpha}.$$

Thus, for $T = 80$ K the current dependence of the power spectral density is expected to be $S_I \propto I^{1.25}$. The calculated exponent c from the nonlinear IV curves according to $c = 2/b$ is represented by the red dashed line in Fig. 13. Although these values fit the data better, the normalization to V^2 should still be valid, which is not the case. It was found that $d \ln S_I/d \ln I$ (filled circles) as well as $d \ln S_I/d \ln V$ (empty circles) show deviations from two. So another possible explanation for the deviations from Hooge's law is that the effect of nonlinear IV curves, i.e., voltage-induced unbinding of thermally excited electron-hole pairs [23], also influences the charge carrier density n . Thus higher voltages lead to an increase in the number of free carriers or changes of the mobility or number of conduction paths due to the current-induced melting of CO domains [17,26]. The increase of n or the noisy volume Ω with the applied electric field then compensates the increase of S_I with the current squared so that the growth is weaker than usual which leads to a decrease in the normalized noise magnitude. To quantitatively analyze the influence of nonlinear IV curves on the resistance fluctuations, we consider the current-dependent resistance $R(I)$ analogous to [34]

$$R(I) = R_0 f(I, c_1, c_2),$$

where R_0 is the resistance for no applied current and f is a function which satisfies $f(0, c_1, c_2) = 1$. The resistance fluctuations $\langle (dR)^2 \rangle / R^2$ can be determined according to

$$\begin{aligned} (dR)^2 &= [(dR_0)f + R_0 df]^2 = (dR_0)^2 f^2 + R_0^2 (df)^2 + 2(dR_0)f R_0 df, \\ \frac{(dR)^2}{R^2} &= \frac{(dR_0)^2}{R_0^2} + \frac{(df)^2}{f^2} + 2 \frac{df}{f} \frac{dR_0}{R_0}, \\ df &= \frac{\partial f}{\partial I} dI + \frac{\partial f}{\partial c_1} dc_1 + \frac{\partial f}{\partial c_2} dc_2, \end{aligned}$$

$$\begin{aligned}
(df)^2 &= \left(\frac{\partial f}{\partial I}\right)^2 (dI)^2 + \left(\frac{\partial f}{\partial c_1}\right)^2 (dc_1)^2 + \left(\frac{\partial f}{\partial c_2}\right)^2 (dc_2)^2 \\
&\quad + 2\left[\frac{\partial f}{\partial I} dI \frac{\partial f}{\partial c_1} dc_1 + \frac{\partial f}{\partial I} dI \frac{\partial f}{\partial c_2} dc_2 + \frac{\partial f}{\partial c_1} dc_1 \frac{\partial f}{\partial c_2} dc_2\right], \\
\frac{(dR)^2}{R^2} &= \frac{(dR_0)^2}{R_0^2} + \left(\frac{\partial \ln f}{\partial I}\right)^2 (dI)^2 + \sum_i \left(\frac{\partial \ln f}{\partial c_i}\right)^2 (dc_i)^2 + 2 \sum_i \frac{\partial \ln f}{\partial I} \frac{\partial \ln f}{\partial c_i} dI dc_i \\
&\quad + \sum_{i \neq j} \frac{\partial \ln f}{\partial c_i} \frac{\partial \ln f}{\partial c_j} dc_i dc_j + 2 \frac{dR_0}{R_0} \left(\frac{\partial \ln f}{\partial I} dI + \sum_i \frac{\partial \ln f}{\partial c_i} dc_i\right).
\end{aligned}$$

Time averaging and assuming an ideal current source, i.e., $\langle (dI)^2 \rangle = 0$, $\langle dI dc_i \rangle = 0$, and $\langle dR_0 dI \rangle = 0$, yields

$$\frac{\langle (dR)^2 \rangle}{R^2} = \frac{\langle (dR_0)^2 \rangle}{R_0^2} + \sum_i \left(\frac{\partial \ln f}{\partial c_i}\right)^2 \langle (dc_i)^2 \rangle + \sum_{i \neq j} \frac{\partial \ln f}{\partial c_i} \frac{\partial \ln f}{\partial c_j} \langle dc_i dc_j \rangle + \frac{2}{R_0} \sum_i \frac{\partial \ln f}{\partial c_i} \langle dR_0 dc_i \rangle.$$

For a specific function $f(I, K, b) = (1 + KI^b)$, which is used to fit the nonlinear IV curves, we get

$$\begin{aligned}
\frac{\langle (dR)^2 \rangle}{R^2} &= \frac{\langle (dR_0)^2 \rangle}{R_0^2} + \left(\frac{\partial \ln f}{\partial K}\right)^2 \langle (dK)^2 \rangle + \left(\frac{\partial \ln f}{\partial b}\right)^2 \langle (db)^2 \rangle + 2 \frac{\partial \ln f}{\partial K} \frac{\partial \ln f}{\partial b} \langle dK db \rangle \\
&\quad + \frac{2}{R_0} \left(\frac{\partial \ln f}{\partial K} \langle dR_0 dK \rangle + \frac{\partial \ln f}{\partial b} \langle dR_0 db \rangle\right), \\
\frac{\langle (dR)^2 \rangle}{R^2} &= \frac{\langle (dR_0)^2 \rangle}{R_0^2} + \frac{I^{2b}}{(KI^b + 1)^2} \langle (dK)^2 \rangle + \frac{K^2 I^{2b} [\ln(I)]^2}{(KI^b + 1)^2} \langle (db)^2 \rangle + 2 \frac{KI^{2b} \ln(I)}{(KI^b + 1)^2} \langle dK db \rangle \\
&\quad + \frac{2}{R_0} \left(\frac{I^b}{KI^b + 1} \langle dR_0 dK \rangle + \frac{KI^b \ln(I)}{KI^b + 1} \langle dR_0 db \rangle\right), \\
\frac{\langle (dR)^2 \rangle}{R^2} &= \frac{\langle (dR_0)^2 \rangle}{R_0^2} + \frac{1}{(K + I^{-b})^2} \{ \langle (dK)^2 \rangle + K^2 [\ln(I)]^2 \langle (db)^2 \rangle + 2K \ln(I) \langle dK db \rangle \} \\
&\quad + \frac{2}{R_0(K + I^{-b})} [\langle dR_0 dK \rangle + K \ln(I) \langle dR_0 db \rangle].
\end{aligned}$$

From this we can see, that the normalized PSD in the ohmic state, $\langle (dR_0)^2 \rangle / R_0^2$, gets only reduced by a negative contribution of the mixed terms in the brackets. This means that there must be a correlation between the parameters dK and db and/or between dR_0 and dK/db .

-
- [1] F. Kagawa and H. Oike, *Adv. Mater.* **29**, 1601979 (2017).
[2] F. Kagawa, T. Sato, K. Miyagawa, K. Kanoda, Y. Tokura, K. Kobayashi, R. Kumai, and Y. Murakami, *Nat. Phys.* **9**, 419 (2013).
[3] T. Sato, F. Kagawa, K. Kobayashi, A. Ueda, H. Mori, K. Miyagawa, K. Kanoda, R. Kumai, Y. Murakami, and Y. Tokura, *J. Phys. Soc. Jpn.* **83**, 083602 (2014).
[4] S. Sasaki, K. Hashimoto, R. Kobayashi, K. Itoh, S. Iguchi, Y. Nishio, Y. Ikemoto, T. Moriwaki, N. Yoneyama, M. Watanabe, A. Ueda, H. Mori, K. Kobayashi, R. Kumai, Y. Murakami, J. Müller, and T. Sasaki, *Science* **357**, 1381 (2017).
[5] J. Hubbard, *Proc. R. Soc. London, Ser. A* **276**, 238 (1963).
[6] H. Seo, J. Merino, H. Yoshioka, and M. Ogata, *J. Phys. Soc. Jpn.* **75**, 051009 (2006).
[7] H. Mori, S. Tanaka, and T. Mori, *Phys. Rev. B* **57**, 12023 (1998).
[8] M. Udagawa and Y. Motome, *Phys. Rev. Lett.* **98**, 206405 (2007).
[9] S. Miyashita and K. Yonemitsu, *Phys. Rev. B* **75**, 245112 (2007).
[10] J. Müller, *ChemPhysChem* **12**, 1222 (2011).
[11] J. Müller and T. Thomas, *Crystals* **8**, 166 (2018).
[12] T. Sato, F. Kagawa, K. Kobayashi, K. Miyagawa, K. Kanoda, R. Kumai, Y. Murakami, and Y. Tokura, *Phys. Rev. B* **89**, 121102(R) (2014).
[13] T. Sato, K. Miyagawa, and K. Kanoda, *J. Phys. Soc. Jpn.* **85**, 123702 (2016).
[14] T. Sato, K. Miyagawa, and K. Kanoda, *Science* **357**, 1378 (2017).
[15] T. Thomas, Y. Saito, Y. Agarmani, T. Thyzel, M. Lonsky, K. Hashimoto, T. Sasaki, M. Lang, and J. Müller, *Phys. Rev. B* **105**, L041114 (2022).
[16] M. Watanabe, Y. Noda, Y. Nogami, and H. Mori, *J. Phys. Soc. Jpn.* **73**, 116 (2004).
[17] P. Alemany, J.-P. Pouget, and E. Canadell, *J. Phys.: Condens. Matter* **27**, 465702 (2015).

- [18] J. H. Scofield, *Rev. Sci. Instrum.* **58**, 985 (1987).
- [19] F. N. Hooge, *Phys. Lett. A* **29**, 139 (1969).
- [20] S. Kogan, *Electronic Noise and Fluctuations in Solids* (Cambridge University Press, Cambridge, 1996).
- [21] B. Hartmann, J. Müller, and T. Sasaki, *Phys. Rev. B* **90**, 195150 (2014).
- [22] Y. Takahide, T. Konoike, K. Enomoto, M. Nishimura, T. Terashima, S. Uji, and H. M. Yamamoto, *Phys. Rev. Lett.* **96**, 136602 (2006).
- [23] Y. Takahide, M. Kimata, K. Hazama, T. Terashima, S. Uji, T. Konoike, and H. M. Yamamoto, *Phys. Rev. B* **81**, 235110 (2010).
- [24] K. Hashimoto *et al.* (unpublished).
- [25] H. Oike, M. Suda, M. Kamitani, A. Ueda, H. Mori, Y. Tokura, H. M. Yamamoto, and F. Kagawa, *Phys. Rev. B* **97**, 085102 (2018).
- [26] Y. Nogami, N. Hanasaki, M. Watanabe, K. Yamamoto, T. Ito, N. Ikeda, H. Ohsumi, H. Toyokawa, Y. Noda, I. Terasaki, H. Mori, and T. Mori, *J. Phys. Soc. Jpn.* **79**, 044606 (2010).
- [27] M. Watanabe, K. Yamamoto, T. Ito, Y. Nakashima, M. Tanabe, N. Hanasaki, N. Ikeda, Y. Nogami, H. Ohsumi, H. Toyokawa, Y. Noda, I. Terasaki, F. Sawano, T. Suko, H. Mori, and T. Mori, *J. Phys. Soc. Jpn.* **77**, 065004 (2008).
- [28] D. Li, A. A. Sharma, D. K. Gala, N. Shukla, H. Paik, S. Datta, D. G. Schlom, J. A. Bain, and M. Skowronski, *ACS Appl. Mater. Interfaces* **8**, 12908 (2016).
- [29] Z. Chen and C. C. Yu, *Phys. Rev. Lett.* **98**, 057204 (2007).
- [30] T. Takahashi, R. Chiba, K. Hiraki, H. M. Yamamoto, and T. Nakamura, *J. Phys. IV* **114**, 269 (2004).
- [31] R. Chiba, K. Hiraki, T. Takahashi, H. M. Yamamoto, and T. Nakamura, *Phys. Rev. Lett.* **93**, 216405 (2004).
- [32] C. Parman and J. Kakalios, *Phys. Rev. Lett.* **67**, 2529 (1991).
- [33] A. Carbone, P. Mazzetti, and F. Rossi, *Appl. Phys. Lett.* **78**, 2518 (2001).
- [34] K. K. Bardhan, C. D. Mukherjee, and U. N. Nandi, *AIP Conf. Proc.* **800**, 109 (2005).
- [35] A. Bid, A. Guha, and A. K. Raychaudhuri, *Phys. Rev. B* **67**, 174415 (2003).
- [36] G. N. Daptary, S. Kumar, M. Kareev, J. Chakhalian, A. Bid, and S. Middey, *Phys. Rev. B* **100**, 125105 (2019).
- [37] M. Watanabe, Y. Noda, Y. Nogami, and H. Mori, *Synth. Met.* **135-136**, 665 (2003).
- [38] J. Müller, J. Brandenburg, and J. A. Schlueter, *Phys. Rev. Lett.* **102**, 047004 (2009).
- [39] H. Oike, F. Kagawa, N. Ogawa, A. Ueda, H. Mori, M. Kawasaki, and Y. Tokura, *Phys. Rev. B* **91**, 041101(R) (2015).
- [40] F. Nad, P. Monceau, and H. M. Yamamoto, *J. Phys.: Condens. Matter* **18**, L509 (2006).
- [41] S. Tomić and M. Dressel, *Rep. Prog. Phys.* **78**, 096501 (2015).
- [42] J. Müller, S. Iguchi, H. Taniguchi, and T. Sasaki, *Phys. Rev. B* **102**, 100103(R) (2020).
- [43] P. Dutta, P. Dimon, and P. M. Horn, *Phys. Rev. Lett.* **43**, 646 (1979).
- [44] T. S. Inada, I. Terasaki, H. Mori, and T. Mori, *Phys. Rev. B* **79**, 165102 (2009).